Spatial Extreme Value Analysis of Extreme Rainfall Using the Extremal-t Process

Husna Mir'atin Nuroini[1*], Sutikno[1], and Purhadi[1]
[1]Department of Statistics, Institut Teknologi Sepuluh Nopember, Surabaya, Indonesia
*Corresponding author: husnamn@its.ac.id

Received: 13 August 2025
Revised: 3 November 2025
Accepted: 28 November 2025

ABSTRACT – **Indonesia's diverse topography, consisting of coasts, lowlands, highlands, and mountains, results in a wide range of weather and climate conditions, enabling various hydrological phenomena such as extreme rainfall, hurricanes, high temperatures, and storms. In recent years, global warming has emerged as a major environmental concern, with one of its significant impacts being climate change. This, in turn, increases the frequency and intensity of extreme hydrological events, potentially causing floods, transportation and communication disruptions, infrastructure damage, agricultural losses, and threats to human life. This study aims to identify the best model and estimate the return levels of extreme rainfall in Ngawi Regency from March 1990 to November 2022 using spatial extreme value analysis with max-stable processes and the extremal-t process. Daily rainfall data from 1990 - 2018 were used for model training, while data from 2018 - 2022 were allocated for model testing to validate predictive performance. Parameter estimation was conducted using Maximum Likelihood Estimation (MLE) and Maximum Pairwise Likelihood Estimation (MPLE), solved through the Broyden-Fletcher-Goldfarb-Shanno (BFGS) Quasi-Newton numerical iteration method. The analysis shows that the best trend surface model has average rainfall and variance influenced by latitude, while the distribution shape is unaffected by latitude or longitude, indicating isotropy. Furthermore, the return level prediction demonstrates higher accuracy when applied over a three-year period.**

Keywords – **Extremal-t Process, Extreme Rainfall, Maximum Pairwise Likelihood Estimation, Max-Stable Processes, Return Level.**

I. INTRODUCTION

Indonesia's geographic position in the tropics, between two continents and two oceans, and crossed by the equator, causes its territory to have a high diversity of weather and climate. In addition, the topographic conditions of Indonesia, which are mountainous, hilly, and coastal areas, become local factors that contribute to the diverse climate conditions [1]. As a result of being crossed by the equator, Indonesia has two seasons alternately on certain months. However, with the advancement of technology, the seasons have shifted and are hard to predict. Nowadays, climate change has become an important issue discussed in environmental problems as one of the impacts of global warming. Climate change is causing changes in rainfall patterns, the length of rainy seasons, shifts in the start of rainy seasons, and an increase in extreme climate events that impact the agricultural sector [2].

In addition, climate change also affects the occurrence of hydrometeorological disasters such as tropical cyclones, thunderstorms, ice storms, extreme rainfall, flooding, frost, and cold temperatures [3], and increases the frequency and intensity of extreme hydrological events [4]. A recent national-scale study based on long-term CHIRPS v2.0 satellite data from 1981 to 2023 revealed significant upward trends in the frequency and intensity of extreme rainfall events across several Indonesian regions, particularly Sulawesi, Maluku, and Papua [5]. Although spatial disparities exist, these findings confirm that Indonesia is experiencing intensifying rainfall extremes, emphasizing the need for localized studies in regions such as Java, including Ngawi to better understand spatial rainfall behavior and anticipate regional climate risks. Furthermore, future projections using 24 global climate models from the Coupled Model Intercomparison Project Phase 6 (CMIP6) indicate that extreme rainfall and prolonged dry periods in Indonesia will intensify throughout the 21st century [6]. These changes are expected to vary seasonally and spatially, with Java projected to experience more frequent and intense rainfall events, posing significant risks to its densely populated areas. These findings underscore the urgency of region-specific studies and risk mitigation strategies in Java.

Extreme events tend to follow certain cycles, yet remain difficult to predict precisely. Therefore, specialized statistical methods are required to analyze such phenomena, particularly extreme rainfall. One such method is Extreme Value Theory (EVT), which has been widely applied in climate studies. As EVT developed, its application expanded into spatial domains to account for the spatial dependence among multiple locations, especially in areas within similar monsoon zones that are assumed to share homogeneous rainfall characteristics. This spatial extension is known as Spatial Extreme Value (SEV) analysis. In SEV, extreme values can be identified through the block maxima and peaks over threshold methods [7], where block maxima data follows the Generalized Extreme Value (GEV) distribution. Spatial modeling of GEV parameters can be performed using Max-Stable Process (MSP) [8], an infinite dimensional extension of the multivariate extreme value distribution [9]. MSP transforms marginal distributions into the Frechet scale and models spatial dependencies. Several approaches have been developed under MSP, including Smith's storm profile, Schlather, Brown-Resnick, geometric Gaussian, and the extremal-t process [10], the latter being an extension of the Schlather model and recently applied in extreme rainfall projection studies [11]. Additionally, large-scale climate phenomena such as the El Niño–Southern Oscillation (ENSO) and the Indian Ocean Dipole (IOD) have been shown to significantly influence spatial patterns of rainfall extremes across Indonesia [12].

Research by [13] modeled extreme rainfall in central Russia by comparing the Schlather, Smith, Brown-Resnick, and extremal-t models, and showed that the extremal-t process with a Whittle-Matern correlation function performed best based on Takeuchi Information Criterion (TIC). Similarly, [14] modeled extreme snow depth in Austria and found that the extremal-t model outperformed other max-stable models, yielding the lowest TIC values. Furthermore, [11] demonstrated that the extremal-t model not only achieved the minimum TIC but also reproduced the spatial dependence of extreme precipitation more accurately than GCM–RCM simulations, showing the lowest RMSE in both summer and winter. These findings reinforce the robustness of the extremal-t process, supporting its application in the current study to model spatial extremes in Indonesian rainfall data. A separate study in the Nelson Churchill River Basin (NCRB) also confirmed that the extremal-t max-stable model effectively captured spatial dependencies of annual maximum precipitation, with topography, coordinates, and even temporal trends (e.g., climate change) proving to be important covariates [15].

The estimation method for the parameters in this research is Maximum Likelihood Estimation (MLE). [16] developed a parameter estimation method for MSP using a likelihood method with a pairwise function called Maximum Pairwise Likelihood Estimation (MPLE). The estimation parameters process with the likelihood method does not always generate closed-form equations, so it needs to be solved by numerical iteration methods, such as Broyden-Fletcher-Goldfarb-Shanno (BFGS) Quasi-Newton which has fast convergence properties. Based on the discussion above, research will be conducted with SEV modeling through the MSP approach using the extremal-t process with BFGS Quasi-Newton numerical iteration method applied to extreme rainfall data from nine observation stations in Ngawi regency in 1990 – 2022.

II. LITERATURE REVIEW

A. Spatial Extreme Value

Applied statistical methods that develop techniques and modeling to describe extreme events is Extreme Value Theory (EVT). One of the key features that distinguish EVT from other analyses is its aim to measure the stochastic behavior of extreme events, both maximum and minimum [17]. In its application, extreme events, especially environmental phenomena, have a spatial aspect, with similarities between events in one location and those in the surrounding area.

Spatial Extreme Value (SEV) is analyzed through Multivariate Extreme Value (MEV), with the spatial aspect is considered a multivariate variable. Then observations will be taken from several neighboring locations. Let $M(s,t)$ represent extreme event data at location s and block period t, in the spatial domain $D \subset \mathbb{R}^2$. The distribution of $M(s,t)$ is shown below.

$$M(s,t) \sim GEV(\mu(s,t), \sigma(s,t), \xi(s,t))$$

where $\mu(s,t), \sigma(s,t), \xi(s,t)$ are the parameter of location, scale, and shape of the GEV distribution.

Cumulative Distribution Function (CDF) for GEV is given in the equation (1) [18].

$$F(y;\mu,\sigma,\xi) = \begin{cases} \exp\left(-\left(1+\xi\left(\frac{y-\mu}{\sigma}\right)\right)^{-\frac{1}{\xi}}\right), \xi \neq 0 \\ \exp\left(-\exp\left(-\frac{y-\mu}{\sigma}\right)\right), \xi = 0 \end{cases} \quad (1)$$

Probability Density Function (PDF) for GEV distribution is shown in the equation (2).

$$f(y;\mu,\sigma,\xi) = \begin{cases} \frac{1}{\sigma}\left(1+\xi\left(\frac{y-\mu}{\sigma}\right)\right)^{-\frac{1}{\xi}-1} \exp\left(-\left(1+\xi\left(\frac{y-\mu}{\sigma}\right)\right)^{-\frac{1}{\xi}}\right), \xi \neq 0 \\ \frac{1}{\sigma}\exp\left(-\frac{y-\mu}{\sigma}\right)\exp\left(-\exp\left(-\frac{y-\mu}{\sigma}\right)\right), \xi = 0 \end{cases} \quad (2)$$

with y is observation variable, μ is parameter of location $(-\infty < \mu < \infty)$, σ is parameter of scale $(\sigma > 0)$, and ξ is parameter of shape $(-\infty < \mu < \infty)$. Based on the shape parameter value, the GEV distribution classified into three types, there are:

a. Type I – Gumbel distribution, if $\xi = 0$
b. Type II – Frechet distribution, if $\xi > 0$
c. Type III – Weibull distribution, if $\xi < 0$

If $\xi > 0$, then extreme values will be distributed to Frechet with PDF as follows.

$$f(y;\mu,\sigma,\xi) = \frac{1}{\sigma}\exp\left(-\left(\frac{y-\mu}{\sigma}\right)^{-\frac{1}{\xi}}\right)\frac{1}{\xi}\left(\frac{y-\mu}{\sigma}\right)^{-\frac{1}{\xi}-1} \tag{3}$$

CDF of Frechet distribution is shown in the equation (4) below.

$$F(y;\mu,\sigma,\xi) = \exp\left(-\left(1+\xi\left(\frac{y-\mu}{\sigma}\right)\right)^{-\frac{1}{\xi}}\right), y > \mu \tag{4}$$

A transformation to the Frechet marginal unit is performed by standardizing Y as Z through equation (5) [16].

$$Z = \left(1+\xi\left(\frac{y-\mu}{\sigma}\right)\right)^{\frac{1}{\xi}} \tag{5}$$

Thus, the CDF of Frechet distribution is obtained in the following equation (6).

$$F(z) = \exp\left(-\frac{1}{z}\right), z > 0 \tag{6}$$

If there are many locations under observations, then MEV analysis becomes difficult because the distribution is low-dimensional or limited. To solve this, the Max-Stable Processes approach is used.

B. Max-Stable Processes

Max-Stable Processes (MSP) generates from the generalization of EVT as an infinite-dimensional extension of MEV, where the observation sample is taken from the maximum value at each spatial process location [9]. MSP transforms the marginal distribution of extreme values into a Fréchet distribution. Let $\{Y_i(s), s \in \mathbb{R}^d, i = 1,2,\dots,n\}$ represent a stochastic process that is independent on the set Y. If there is a series of continuous function $a_n(s) > 0$ and $b_n(s) \in \mathbb{R}$, so that

$$Z(s) = \lim_{n\to\infty} \frac{\max_{i=1} Y_i(s) - b_n(s)}{a_n(s)}, n \to \infty, s \in \mathbb{R}^d$$

Hence the stochastic process $\{Z(s), s \in \mathbb{R}^d\}$ is MSP [19]. If $a_n(s) = n$ and $b_n(s) = 0$, then $Z(s)$ is simple MSP with Frechet marginal unit that explained through the following equation.

$$Z(s) = \max_{i\geq 1}\{U_i W_i(s)\}, s \in S$$

where $\{U_i\}$ are infinite number of points of Poisson process on $(0,\infty) \times \mathbb{R}^d$ with measurement intensity $d\Lambda(U) = U^{-2}dU$, and $W_i(s)$ are independent realizations of a non-negative stochastic process $W(s)$. The general equation for Max-Stable Processes can be formulated into several approaches, there are Smith, Schlather, Brown-Resnick, Gaussian geometric, and extremal-t.

C. Extremal-t Process

Extremal-t is a family of Max-Stable Processes that stems from the development of Schlather. A stationary Max-Stable Processes with a Frechet marginal unit for extremal-t is defined in the following equation [10].

$$Z(s) = c_r \max_{i\geq 1}\{U_i V_i(s)^r\}, r \geq 1, s \in S$$

where $c_r = \pi^{1/2}2^{-(r-2)/2}\Gamma\big((r+1)/2\big)^{-1}$, $\{U_i\}$ is infinite number of points of Poisson process on $(0,\infty) \times \mathbb{R}^d$, $V(s)$ is a standard Gaussian process with correlation function ρ, and Γ represent gamma function.

The bivariate CDF of extremal-t process is shown in the equation (7) below [20].

$$F(z_{ji}, z_{ki}) = \exp\left[-\frac{1}{z_{ji}}T_{r+1}\left(-\frac{\rho(h)}{b}+\frac{1}{b}\left(\frac{z_{ki}}{z_{ji}}\right)^{\frac{1}{r}}\right)-\frac{1}{z_{ki}}T_{r+1}\left(-\frac{\rho(h)}{b}+\frac{1}{b}\left(\frac{z_{ji}}{z_{ki}}\right)^{\frac{1}{r}}\right)\right] \tag{7}$$

where T_{r+1} is CDF of univariate Student-t distribution with degree of freedom $r+1$ and $b^2 = \frac{(1-\rho(h)^2)}{(r+1)}$

This research uses correlation functions for spatial data based on distance measurements. There are several correlation functions $(\rho(h))$ that come from the parametric family that can be used, such as Whittle-Matern, Cauchy, powered exponential, and Bessel [19].

D. Block Maxima

Generally, there are two ways to identify extreme values, using block maxima and peaks over threshold. The block maxima method is performed by selecting the maximum value of a variable grouped into several blocks based on a certain period, such as months or years. The selected values from each block are the extremes.

The block maxima method is based on the classical extreme value theorem, which states that the maximum of a sequence of independent and identically distributed random variables converges to a Generalized Extreme Value (GEV) distribution [21], [22]. If there are constants $a_n > 0$ and b_n such that,

$$P\left(\frac{M_n - b_n}{a_n} \leq y\right) \rightarrow G(y) \text{ when } n \rightarrow \infty$$

where $M_n = max\{Y_1, Y_2, \dots, Y_n\}$ and G is a non-degenerate distribution function. There are three possible distributions for G: Gumbel, Frechet, or Weibull. The generalization of these three distributions is the Generalized Extreme Value (GEV) [7].

E. Maximum Likelihood Estimation (MLE)

The parameters of GEV distribution can be estimated through several methods, one of them is using MLE. The main principle of MLE is to maximize the likelihood function of the GEV distribution's PDF, where the likelihood function is the joint probability function of $y_1, y_2, \dots, y_n$. Based on the MLE method, the likelihood function for GEV in the equation (2) with $\xi \neq 0$ can be shown through equation (8) below.

$$L(\mu, \sigma, \xi) = \prod_{i=1}^{n} f(y_i; \mu, \sigma, \xi) \tag{8}$$

The likelihood function in equation (8) is denoted as $L(\mu, \sigma, \xi) = L(\boldsymbol{\theta})$, where $\boldsymbol{\theta} = [\mu \quad \sigma \quad \xi]^T$. The next step is maximizing the likelihood function by taking the ln form of equation (8), then calculating the first derivative of the ln likelihood function for each parameter, and equating it to zero.

Necessary conditions : $\frac{\partial \ln(L(\boldsymbol{\theta}))}{\partial \boldsymbol{\theta}} = 0,$ so obtained $\widehat{\boldsymbol{\theta}}$

Sufficient conditions : $\frac{\partial^2 \ln(L(\boldsymbol{\theta}))}{\partial \boldsymbol{\theta}\, \partial \theta^T} = \boldsymbol{H}(\boldsymbol{\theta}),$ that is called Hessian matrix.

F. Maximum Pairwise Likelihood Estimation (MPLE)

The method for estimating parameters in MSP uses a pairwise density function that is analyzed through MPLE [23]. The parameter estimation result of MPLE will be used to arrange trend surface models in the form of multiple regression equations with longitude and latitude as explanatory variables. The trend surface model is expressed in the following equation (9).

$$\begin{aligned} \mu(s) &= \beta_{0,\mu} + \beta_{1,\mu} u(s) + \beta_{2,\mu} v(s) \\ \sigma(s) &= \beta_{0,\sigma} + \beta_{1,\sigma} u(s) + \beta_{2,\sigma} v(s) \\ \xi(s) &= \beta_{0,\xi} \end{aligned} \tag{9}$$

Furthermore, equation (9) is written into matrix form as follows.

$$\mu(s) = \boldsymbol{d}^T \boldsymbol{\beta}_{\boldsymbol{\mu}} \qquad \sigma(s) = \boldsymbol{d}^T \boldsymbol{\beta}_{\boldsymbol{\sigma}} \qquad \xi(s) = \beta_{\xi} = \beta_{0,\xi}$$

where,

$\boldsymbol{d}^T = [1 \quad u(s) \quad v(s)]$, $\boldsymbol{\beta_\mu} = [\beta_{0,\mu} \quad \beta_{1,\mu} \quad \beta_{2,\mu}]$ $\boldsymbol{\beta_\sigma} = [\beta_{0,\sigma} \quad \beta_{1,\sigma} \quad \beta_{2,\sigma}]$

$u(s)$ = Longitude of location s

$v(s)$ = Latitude of location s

The parameter of $\boldsymbol{\beta}$, where $\boldsymbol{\beta} = [\boldsymbol{\beta}_\mu^T \quad \boldsymbol{\beta}_\sigma^T \quad \beta_\xi]^T$ is estimated according to the PDF of each MSP approach through MPLE method by replacing $L(\boldsymbol{\beta})$ function in MLE with the pairwise likelihood function $L_p(\boldsymbol{\beta})$ in equation (10).

$$L(\boldsymbol{\beta}) = \prod_{i=1}^{n} \prod_{j=1}^{m-1} \prod_{k=j+1}^{m} f(y_{ji}, y_{ki}; \boldsymbol{\beta}) \tag{10}$$

where $f(y_{ji}, y_{ki}; \boldsymbol{\beta})$ is bivariate PDF with $\boldsymbol{\beta}$ parameter and $i = 1,2, \dots, n$ is observations on each variable.

The parameter estimation of $\boldsymbol{\beta}$ can be obtained when the likelihood function is formed according to $f(y_{ji}, y_{ki})$. Therefore, the function of $f(y_{ji}, y_{ki}; \boldsymbol{\beta})$ needs to be formed first using $f(z_{ji}, z_{ki})$ through equation (11).

$$f_{Y_{ji},Y_{ki}}(y_{ji}, y_{ki}; \boldsymbol{\beta}) = f(z_{ji}, z_{ki}) |J(y_{ji}, y_{ki})| \tag{11}$$

where,

$$|J(y_{ji}, y_{ki})| = \frac{1}{\sigma_{ji}\, \sigma_{ki}} \left(1 + \xi_{ji} \left(\frac{y_{ji} - \mu_{ji}}{\sigma_{ji}}\right)\right)^{\frac{1}{\xi_{ji}} - 1} \left(1 + \xi_{ki} \left(\frac{y_{ki} - \mu_{ki}}{\sigma_{ki}}\right)\right)^{\frac{1}{\xi_{ki}} - 1}$$

G. Broyden-Fletcher-Goldfarb-Shanno (BFGS) Quasi-Newton

Maximum Likelihood Estimation (MLE) for this model does not yield parameter estimates in closed form, requiring a numerical iterative procedure. Among various optimization algorithms, the BFGS Quasi-Newton method is widely used and is named after its developers Broyden, Fletcher, Goldfarb, and Shanno [19]. The Newton method itself updates parameters using derivative information derived from a Taylor series expansion. The iteration formula for the BFGS Quasi-Newton method is given as follows.

$$\boldsymbol{\beta}^{(k+1)} = \boldsymbol{\beta}^{(k)} + \alpha^{(k)} \boldsymbol{s}(\boldsymbol{\beta}^{(k)}) \tag{12}$$

where $\alpha^{(k)}$ is the step size that minimizes the objective function.

$$\alpha^{(k)} = \arg\min \left(f\left(\boldsymbol{\beta}^{(k)} + \alpha^{(k)} \boldsymbol{s}(\boldsymbol{\beta}^{(k)})\right)\right) = \frac{\boldsymbol{s}(\boldsymbol{\beta}^{(k)})}{\boldsymbol{s}(\boldsymbol{\beta}^{(k)})^T \boldsymbol{H}(\boldsymbol{\beta}^{(k)}) \boldsymbol{s}(\boldsymbol{\beta}^{(k)})}$$

$$\boldsymbol{s}(\boldsymbol{\beta}^{(k)}) = -\boldsymbol{H}(\boldsymbol{\beta}^{(k)})^{-1} \boldsymbol{g}(\boldsymbol{\beta}^{(k)})$$

$\boldsymbol{\beta}^{(k)}$: initial value, starting with $k = 0$

$\boldsymbol{H}(\boldsymbol{\beta}^{(k)})^{-1}$: inverse of Hessian matrix

$\boldsymbol{g}(\boldsymbol{\beta}^{(k)})$: vector whose elements contain the first derivatives of the ln likelihood function for each parameter

In the BFGS Quasi-Newton method, the Hessian matrix $\boldsymbol{H}(\boldsymbol{\beta}^{(k)})$ is replaced with an estimation that is a positive definite matrix and has similar properties to the Hessian matrix $\boldsymbol{H}(\boldsymbol{\beta}^{(k)})$.

$$\boldsymbol{H}(\boldsymbol{\beta}^{(k+1)}) = \boldsymbol{H}(\boldsymbol{\beta}^{(k)}) + \left(1 + \frac{\Delta \boldsymbol{g}(\boldsymbol{\beta}^{(k)})^T \boldsymbol{H}(\boldsymbol{\beta}^{(k)}) \Delta \boldsymbol{g}(\boldsymbol{\beta}^{(k)})}{\Delta \boldsymbol{g}(\boldsymbol{\beta}^{(k)})^T \Delta \boldsymbol{\beta}^{(k)}}\right) \frac{\Delta \boldsymbol{\beta}^{(k)} \Delta(\boldsymbol{\beta}^{(k)})^T}{\Delta(\boldsymbol{\beta}^{(k)})^T \Delta \boldsymbol{g}(\boldsymbol{\beta}^{(k)})}$$

$$- \frac{\boldsymbol{H}(\boldsymbol{\beta}^{(k)}) \Delta \boldsymbol{g}(\boldsymbol{\beta}^{(k)}) \Delta(\boldsymbol{\beta}^{(k)})^T + \left(\boldsymbol{H}(\boldsymbol{\beta}^{(k)}) \Delta \boldsymbol{g}(\boldsymbol{\beta}^{(k)}) \Delta(\boldsymbol{\beta}^{(k)})^T\right)^T}{\Delta \boldsymbol{g}(\boldsymbol{\beta}^{(k)})^T \Delta \boldsymbol{\beta}^{(k)}}$$

Iteration is done until $\|\boldsymbol{\beta}^{(k+1)} - \boldsymbol{\beta}^{(k)}\| \leq e$ where e is a very small number. The first step in the BFGS Quasi-Newton method is arranging the second derivative of ln likelihood function for each parameter and taking the derivative of the ln likelihood function for the combination parameter.

H. Anderson-Darling Test

An extreme event can be considered max-stable if and only if it follows a Generalized Extreme Value (GEV) distribution. To verify this, a goodness-of-fit test was performed using the Anderson-Darling test under the following hypotheses [24].

$H_0: F(Y) = F^*(Y)$ (Data follows GEV distribution)

$H_1: F(Y) \neq F^*(Y)$ (Data does not follow GEV distribution)

$$A^2 = -\frac{\sum_{i=1}^{n}\left((2i-1)\left(\ln F^*(y_i) + \ln\left(1 - F^*(y_{n+1-i})\right)\right)\right)}{n} - n \tag{13}$$

where,

$F(Y)$: cumulative distribution function of sample data

$F^*(Y)$: theoretical cumulative distribution function

n : sample size

Test criteria: with a significance level of α, the decision will reject H_0 if the value of $A^2 > A^2_{table}$ or $\text{p} - \text{value} < \alpha$.

I. Spatial Dependency

Measuring spatial dependency in extreme data can be done through the extremal coefficient $\theta_{(h)}$ and madogram. The extremal coefficient value of $\theta_{(h)} \in [1,2]$ indicates a measure of the strength of spatial dependence, where $\theta_{(h)} = 1$ it is fully dependent, while $\theta_{(h)} = 2$ it is independent. The extremal coefficient for the extremal-t process depends on the value of r [25]. The paired extremal coefficients for the extremal-t process are defined by Equation (9) below [20].

$$\theta_{(h)} = 2T_{r+1}\left(\sqrt{\frac{r+1}{1-\rho(h)^2}} - \sqrt{\frac{1-\rho(h)^2}{r+1}}\rho(h)\right) \tag{14}$$

$T_r(.|\mu, \xi)$ is the CDF of the student-t distribution with parameters of μ, ξ, r (location, shape, and independent degree parameters, respectively).

The madogram requires the first moment to be infinite which is not always the case for extreme data, to overcome this [26] introduced a modified madogram by transforming the random variable using the extreme value distribution function. If is max-stable stationary with Frechet distribution, then its F-madogram is defined as follows.

$$v_F(h) = \frac{1}{2|N(h)|}\sum_{j=1}^{N(h)}\left|F\left(Z(s_j + h)\right) - F\left(Z(s_j)\right)\right| \tag{15}$$

where $v_F(h)$ is the F-madogram at lag h, s_j is the location of the j^{th} observation point, $Z(s_j)$ is the observation value at the s_j, h is the distance between two locations, $(s_j, s_j + h)$ is the pair of data that is h apart, and $N(h)$ is the number of pairs of locations that are h apart. The relationship between the extremal coefficient and the F-madogram can be seen in the following equation [26].

$$2v_F(h) = \frac{\theta(h) - 1}{\theta(h) + 1}$$

If the value of $\theta_{(h)} \in [1,2]$, then the value of $v_F(h)$ will be in the range of 0 to 0.167. The value of $v_F(h) = 0$ indicates that there is full dependency between pairs of locations, while $v_F(h) = 0.167$ are independent.

J. Takeuchi Information Criterion

The estimation parameter of max-stable processes generates the value of $\hat{\boldsymbol{\beta}}$ that is used to form trend surface model as a linier model of combination of longitude and latitude coordinate of a location with parameter of $\boldsymbol{\beta}$. Selection of the best model based on the smallest TIC value with the following equation [16].

$$TIC = -2\ell_p(\hat{\boldsymbol{\beta}}) + 2tr\left(\boldsymbol{H}(\hat{\boldsymbol{\beta}})^{-1}\boldsymbol{J}(\hat{\boldsymbol{\beta}})\right) \tag{16}$$

$\ell_p(\hat{\boldsymbol{\beta}})$ is ln pairwise likelihood function of $\sum_{i=1}^{n}\sum_{j=1}^{m-1}\sum_{k=j+1}^{m}\ln\left(f(z_{ji}, z_{ki}; \hat{\boldsymbol{\beta}})\right)$; $\boldsymbol{H}(\hat{\boldsymbol{\beta}})$ is Hessian matrix; $-\boldsymbol{H}^{-1}(\hat{\boldsymbol{\beta}})$ shows the variance of parameter vector which is estimated, and J is square score statistic.

K. Significance Test

Test of statistical significance parameter that fitted to spatial data is Wald test. This test can be used int the significance of the model coefficient partially with the following hypothesis [27].

$H_0: \beta_q = 0$ (Parameter is not significant)

$H_1: \beta_q \neq 0$, with $q = \mu, \sigma, \xi$ (Parameter is significant)

$$Wald_q = \frac{\hat{\beta}_q^2}{\widehat{var}(\hat{\beta}_q)} \underset{n\to\infty}{\sim} \chi_1^2 \tag{17}$$

$\widehat{var}(\hat{\beta}_q)$ is major diagonal of matrix $\widehat{var}(\widehat{\boldsymbol{\beta}}) \cong -\boldsymbol{H}^{-1}(\widehat{\boldsymbol{\beta}})$, where $\boldsymbol{H}(\widehat{\boldsymbol{\beta}})$ is second derivative of ln pairwise likelihood function of $\widehat{\boldsymbol{\beta}}$ estimation. Decision criteria: H0 is rejected if value of $Wald_q > \chi^2_{(\alpha,1)}$ or p-value < α.

L. Return Level

Return level is the expected value to be achieved in the upcoming period [11]. This value indicates the probability of an extreme event occurring within a certain period. The return level at location s is denoted by $z_p(s)$ that estimated through equation (18).

$$z_p(s) = \hat{\mu}(s) - \frac{\hat{\sigma}(s)}{\hat{\xi}(s)}\left(1 - \left(-\ln\left(1 - \frac{1}{T}\right)\right)^{-\hat{\xi}(s)}\right) \tag{18}$$

T is return period in years; $\hat{\mu}(s), \hat{\sigma}(s), \hat{\xi}(s)$ is estimation value of location, scale, and shape parameter at location s.

M. Root Mean Square Error

Root Mean Square Error (RMSE) is used as a measure of the goodness of the parameter estimation results. This measurement is carried out by calculating the difference between estimation value and the actual value obtained from the testing data. RMSE can be calculated through the following equation [28].

$$RMSE = \sqrt{\frac{\sum_{j=1}^{m}(y_j - \hat{y}_j)^2}{m}} \tag{19}$$

where,

y_j : actual value of rainfall

$\hat{y}_j$: prediction value

m : number of locations

N. Extreme Rainfall

Extreme rainfall refers to precipitation with an intensity that exceeds the usual upper limit observed at a given location within specific time units, such as minutes, hours, days, or months. Such events are typically associated with the development of large cumulonimbus clouds that extend into the upper atmosphere. These clouds may also be accompanied by strong winds, hail, and even tornadoes [3]. The wet climate in Indonesia is classified into three types of rainfall patterns, such as tropical monsoonal climate, equatorial climate, and local climate [29].

O. Seasonal Zones (ZOM)

Climatologically, the territory of Indonesia can be classified according to the distribution pattern of the average monthly rainfall into:

a. Areas that have climatologically clear boundaries between the wet and dry seasons are called the seasonal zone (ZOM).
b. Areas that do not have clear climatological boundaries between the wet and dry seasons are called non seasonal zones (Non-ZOM).

III. METHODOLOGY

A. Data Source

This study employed the Max-Stable Processes method, specifically the extremal-t process approach, to model extreme rainfall in Ngawi Regency. Daily rainfall data were obtained from the Meteorology, Climatology, and Geophysics Agency (BMKG) for the period March 1990 to November 2022, recorded at nine observation stations: Gemarang, Guyung, Kedungprahu, Kendal, Kricak, Legundi, Paron, Tretes, and Widodaren. Extreme events were identified using the block maxima method, resulting in data that follow the Generalized Extreme Value (GEV) distribution.

The dataset was divided into two subsets:

a. Training data: daily rainfall from 1990–2018, used for model estimation.
b. Testing data: daily rainfall from 2018–2022, used for model validation.

B. Step of Analysis

The analysis was carried out through the following steps:

1. Descriptive statistical analysis to explore the characteristics and patterns of rainfall in Ngawi Regency.
2. Distribution identification for each station to detect heavy-tailed behavior and extreme values using histograms.
3. Extreme value extraction using the block maxima method, grouping the data into four seasonal blocks: December–January–February (DJF), March–April–May (MAM), June–July–August (JJA), and September–October–November (SON).
4. Parameter estimation of the univariate GEV distribution.
5. Goodness-of-fit testing of the GEV distribution using the Anderson–Darling test.
6. Transformation to the Fréchet distribution.
7. Spatial dependence analysis using the extremal coefficient plot and F-madogram plot.
8. Bivariate GEV parameter estimation for extreme rainfall data using Maximum Pairwise Likelihood Estimation.
9. Trend surface model selection by comparing candidate models and choosing the one with the smallest Takeuchi Information Criterion (TIC) value.
10. Parameter significance testing using the Wald test.
11. Prediction of extreme rainfall at each observation station for specified periods by calculating the return level.
12. Model accuracy assessment by calculating the RMSE between the predicted return levels and the testing data.

IV. RESULTS AND DISCUSSIONS

A. Description of Rainfall in Ngawi Regency

Daily rainfall data in Ngawi can be described through descriptive statistical analysis as shown in Table 1. Most observation stations have rainfall of around 4.669 mm/day – 6.069 mm/day, with the highest average intensity being at Kendal station.

Table 1 Descriptive Statistics of Daily Rainfall

Observation Stations	Minimum	Maximum	Mean	Std. Deviation
Gemarang	0	160	4.963	13.697
Guyung	0	168	5.860	15.856
Kedungprahu	0	151	4.669	12.881
Kendal	0	158	6.069	14.928
Kricak	0	156	5.128	12.83
Legundi	0	201	6.054	15.698
Paron	0	190	5.143	14.349
Tretes	0	185	4.685	13.074
Widodaren	0	282	5.858	15.668

According to BMKG, extreme rainfall occurs when daily rainfall intensity exceeds 150 mm/day. As indicated by the maximum daily rainfall values in Table 1, all observation stations in Ngawi Regency recorded intensities above this threshold. The variability of rainfall intensity at each station can be identified through the standard deviation values. Guyung Station exhibits the highest variability, with a standard deviation of 15.856, indicating that daily rainfall at this station fluctuates more widely compared to the other stations. A visual depiction of the rainfall distribution is presented in the histogram below.

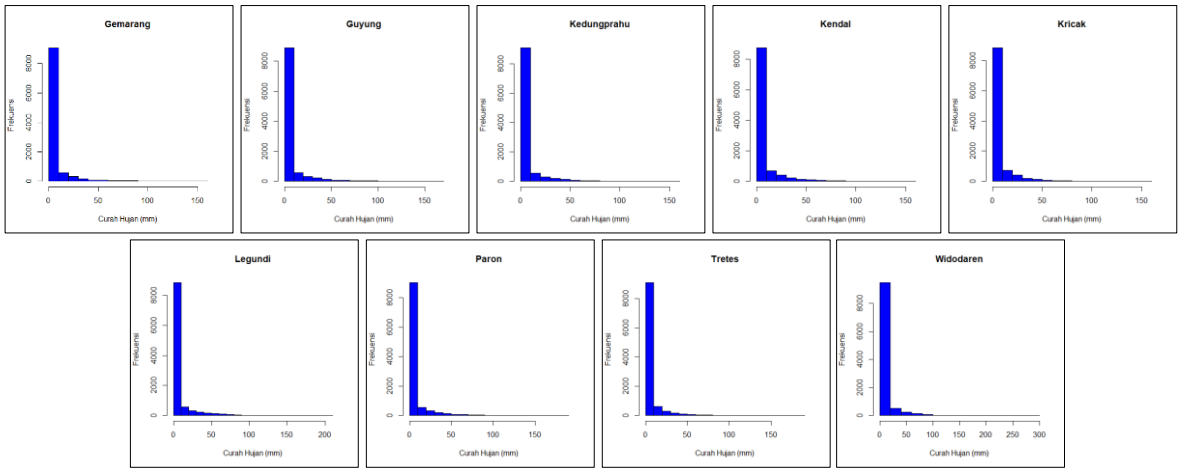

Figure 1 Histogram of Daily Rainfall

Figure 1 shows that the distribution curve is right-skewed, with a high concentration of observations near zero. This pattern indicates a heavy-tailed distribution, making the data appropriate for analysis using Extreme Value Theory (EVT).

B. Identification of Extreme Values using Block Maxima

Extreme value identification in this study was performed using the block maxima method. Based on the monsoonal rainfall pattern in Ngawi Regency, blocks were defined as three-month periods: December–January–February (DJF), March–April–May (MAM), June–July–August (JJA), and September–October–November (SON). The training data were segmented into blocks from March 1990 to November 2018, resulting in a total of 115 blocks. From each block, the maximum rainfall value was extracted as the sample.

C. Estimation Parameter of Univariate GEV

Selected extreme data samples will be analyzed to estimate parameters at each observation station using the MLE method. The results of the univariate GEV parameter estimation are presented in Table 2.

Table 2 Parameter Estimation of Univariate GEV

Observation Stations	$\hat{\mu}(s)$	$\hat{\sigma}(s)$	$\hat{\xi}(s)$
Gemarang	52.114	34.865	-0.251
Guyung	59.730	40.717	-0.343
Kedungprahu	44.502	33.978	-0.266
Kendal	60.619	35.830	-0.307
Kricak	47.472	32.464	-0.214
Legundi	51.235	36.234	-0.169
Paron	53.285	37.303	-0.202
Tretes	47.381	36.189	-0.141
Widodaren	58.210	32.222	-0.081

Parameter $\mu(s)$ indicates the central tendency of the data. The estimated value is highest at Kendal station, which means that the intensity of extreme rainfall at this station tends to be greater than at other stations. Parameter $\sigma(s)$ represents the variability of the data, with Guyung Station having the largest variability value. In addition, the shape parameter $\xi(s)$ describes the right-tail behavior of the data distribution. A greater $\xi(s)$ value indicates a more slowly decaying right tail, resulting in a thicker (heavy) tail. A heavy tail in data distribution increases the likelihood of extreme rainfall events. All observation stations have $\xi < 0$, which requires a transformation to the Frechet distribution ($\xi > 0$).

D. Goodness of Fit Test for Distribution

Extreme rainfall can be analyzed using MSP if the data follows a GEV distribution. Therefore, it is necessary to test the goodness of fit of the data distribution using the Anderson-Darling test with the following hypothesis. The results of the goodness of fit test are presented in Table 3.

Table 3 Anderson-Darling Test

Observation Stations	A^2	$A^2{}_{0.025}$	Decision
Gemarang	0.735	3.078	Failed to Reject H_0
Guyung	0.926	3.078	Failed to Reject H_0
Kedungprahu	1.428	3.078	Failed to Reject H_0
Kendal	0.933	3.078	Failed to Reject H_0
Kricak	0.646	3.078	Failed to Reject H_0
Legundi	1.363	3.078	Failed to Reject H_0
Paron	0.531	3.078	Failed to Reject H_0
Tretes	0.943	3.078	Failed to Reject H_0
Widodaren	2.251	3.078	Failed to Reject H_0

The decision was made by comparing the calculated A^2 coefficients with the critical value. With a significance level of α = 2.5% and the number of observations n = 115, the critical value $A^2{}_{0.025}$ was found to be 3.078. Therefore, it can be concluded that the extreme rainfall data at each station follow the GEV distribution.

E. Measurement of Spatial Dependence

Extreme rainfall is considered spatial data. Therefore, its analysis involves measuring spatial dependence between locations. Closer proximity is assumed to result in stronger dependence. Pairwise spatial dependence was measuriner using extremal coefficients and the F-madogram, which are presented graphically in Figure 2.

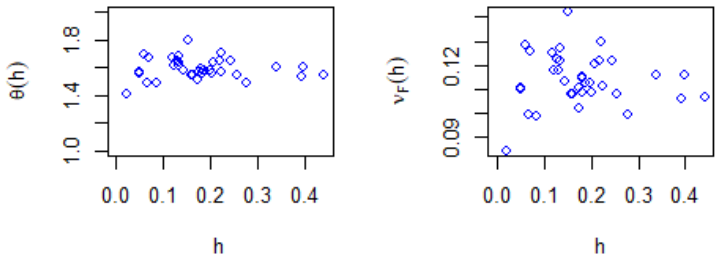

Figure 2 Extremal Coefficients and F-Madogram

Figure 2 shows that the values of $\theta(h)$ range from 1.4 to 1.8, indicating spatial dependence between rainfall observation stations. In addition, $v_F(h)$ values ranging from 0 to 0.14 also indicate spatial dependence between location pairs.

F. Transformation to Frechet Distribution

The MSP analysis was conducted by transforming the data from the GEV distribution to the Frechet distribution. This transformation aims to produce heavy-tailed data, where a fatter tail implies a greater likelihood of extreme events. The transformation results were calculated univariately for each observation station.

G. Parameter Estimation of SEV Using Extremal-t Process

Parameter estimation in the extremal-t process was performed using the MPLE method. However, it resulted in an equation without a closed form. Therefore, the procedure was continued with the BFGS Quasi-Newton numerical iteration. Analysis with the extremal-t process requires correlation functions in the modeling stage, including Whittle-Matern, Cauchy, powered exponential, and Bessel. The best correlation function was selected based on the smallest TIC value, as presented in Table 4.

Table 4 Correlation Function

Correlation Function	TIC
Whittle-Matern	34569.08
Powered exponential	34567.52
Cauchy	34566.10
Bessel	NA

Table 4 shows that the Cauchy correlation function has a smaller TIC value compared to other correlation functions. The NA value indicates the TIC could not be calculated. Therefore, parameter estimation in the extremal-t process was performed using the Cauchy correlation function. The estimation results are required to construct a combination of trend surface models with explanatory variables in the form of longitude and latitude coordinates. The best trend surface model was selected based on the smallest TIC value, obtained through the BFGS Quasi-Newton numerical iteration, as presented in Table 5.

Table 5 Combination of Trend Surface Model

No.	Model	TIC
1	$\hat{\mu}(s) = -6.7749 - 0.0116\ u(s) - 1.2316\ v(s)$ $\hat{\sigma}(s) = 8.6467 + 0.0544\ u(s) + 1.8204\ v(s)$ $\hat{\xi}(s) = 0.6699$	36740.76
2	$\hat{\mu}(s) = -4.6441 + 0.0519\ u(s)$ $\hat{\sigma}(s) = 7.9107 + 0.2486\ \mathrm{u}(s) + 4.5994\ v(s)$ $\hat{\xi}(s) = 0.6586$	37431.24
3	$\hat{\mu}(s) = -5.3229 + 0.1803\ \mathrm{u}(s)$ $\hat{\sigma}(s) = 8.289 - 7.423\ v(s)$ $\hat{\xi}(s) = 4.316$	48569.41
4	$\hat{\mu}(s) = -2.358 - 9.784\ v(s)$ $\hat{\sigma}(s) = 7.735 + 3.645\ u(s) + 8.637\ v(s)$ $\hat{\xi}(s) = 4.877$	60810.85

Several combinations of trend surface models are not shown in Table 5 because their TIC values could not be calculated. Based on the analysis, the best trend surface model is the first combination, with a TIC value of 36740.76, as follows:

$$\hat{\mu}(s) = -6.7749 - 0.0116\, u(s) - 1.2316\, v(s)$$
$$\hat{\sigma}(s) = 8.6467 + 0.0544\, u(s) + 1.8204\, v(s)$$
$$\hat{\xi}(s) = 0.6699$$

After selecting the best trend surface model, the parameter estimates $\hat{\mu}(s)$, $\hat{\sigma}(s)$, and $\hat{\xi}(s)$ for each rainfall observation station were calculated. The estimated values were also used to predict events in future periods through return level analysis.

Table 6 Parameter Estimation of Extremal-t Process

Observation Stations	$\hat{\mu}(s)$	$\hat{\sigma}(s)$	$\hat{\xi}(s)$
Gemarang	1.0470	1.2386	0.6699
Guyung	1.1813	1.0418	0.6699
Kedungprahu	1.1089	1.1418	0.6699
Kendal	1.2497	0.9361	0.6699
Kricak	1.0448	1.2410	0.6699
Legundi	1.1235	1.1348	0.6699
Paron	1.0969	1.1659	0.6699
Tretes	1.1194	1.1244	0.6699
Widodaren	1.0346	1.2516	0.6699

Table 6 presents the estimation results of the extremal-t process parameters for the nine rainfall observation stations in Ngawi District. The shape parameter $\hat{\xi}(s)$ has a constant value because it is assumed to be isotropic, meaning that rainfall characteristics are homogeneous regardless of other factors such as temperature, humidity, wind direction, or altitude.

H. Parameter Significancy Test

The significance test was conducted on the parameters of the best trend surface model. This test requires the variance of each estimated parameter, which can be obtained from the standard error. The results of the $\boldsymbol{\beta}$ parameter significance test are presented in Table 7.

Table 7 Wald Test

Parameter	Coefficient	Std. Error	Wald	$\chi^2_{0.05;1}$	Decision
$\hat{\beta}_{0,\mu}$	–6.7749	18.73	0.1308	3.841	Failed to Reject H_0
$\hat{\beta}_{1,\mu}$	–0.0116	0.163	0.005	3.841	Failed to Reject H_0
$\hat{\beta}_{2,\mu}$	–1.2316	0.52	5.6095	3.841	Reject H_0
$\hat{\beta}_{0,\sigma}$	8.6467	22.47	0.1481	3.841	Failed to Reject H_0
$\hat{\beta}_{1,\sigma}$	0.0544	0.2016	0.0728	3.841	Failed to Reject H_0
$\hat{\beta}_{2,\sigma}$	1.8204	0.4959	13.475	3.841	Reject H_0
$\hat{\beta}_{0,\xi}$	0.6699	0.0306	480.84	3.841	Reject H_0

The decision was made by comparing the calculated Wald coefficient with the critical value $\chi^2_{0.05;1} = 3.841$. Based on Table 7, with a significance level of $\alpha = 5\%$, the parameters that have a significant partial effect on the trend surface model are $\hat{\beta}_{2,\mu}$, $\hat{\beta}_{2,\sigma}$, and $\hat{\beta}_{0,\xi}$. Therefore, it can be concluded that each observation station has a different average rainfall and variability according to its latitude coordinates, while the tail behavior of the data distribution is the same across stations regardless of latitude or longitude.

I. Return Level

The prediction of extreme rainfall in a certain time period can be calculated through return levels. The calculation requires parameter estimation values $\hat{\mu}(s), \hat{\sigma}(s),\ and\ \hat{\xi}(s)$ obtained from the trend surface model. This research makes predictions for the next 1, 2, 3, and 4 years, where the first year consists of 4 blocks so that the period value T = 4. Furthermore, the second to fourth years use T = 8, T = 12, and T = 16, respectively. The probability of the return level value obtained is 1/T. The results of the extremal-t process return level calculation are presented in Table 8.

Table 8 Return Level

Observation Stations	1 Year	2 Years	3 Years	4 Years
Gemarang	89.284	103.576	110.283	114.557
Guyung	98.854	112.748	119.232	123.322
Kedungprahu	79.485	92.808	99.115	103.143
Kendal	94.628	107.105	113.156	117.045
Kricak	82.860	96.950	103.675	108.001
Legundi	90.691	107.030	115.130	120.439
Paron	93.450	109.643	117.510	122.612
Tretes	87.230	104.257	112.811	118.463
Widodaren	96.364	113.610	122.352	128.178

The return level values in Table 8 indicate an upward trend in predicted extreme rainfall across periods. The highest return level is at Widodaren Station, with a rainfall intensity of 128.178 mm/day, expected to occur between the first year to the fourth year. The probability of this event is $p = \frac{1}{T} = \frac{1}{16} = 0.0625 = 6.25\%$. If the return level at Widodaren Station is calculated for the next one-year period, a lower return level value of 96.364 mm/day is obtained, with a 25% probability of occurrence. Nevertheless, the occurrence of rainfall with an intensity of 128.178 mm/day should still be taken into consideration.

J. Model Goodness Measurement

The goodness of fit of the model was evaluated using the Root Mean Square Error (RMSE), which quantifies the deviation between the actual and the predicted values. A smaller RMSE indicates a better model, as it means the predictions are closer to the observed data. The RMSE values for extreme rainfall predictions for return periods of 1, 2, 3, and 4 years are presented as follows.

Table 9 Comparison Between Actual and Predicted Values

Observation Stations	2019		2020	
	Actual	Predicted	Actual	Predicted
Gemarang	45	89.284	80	103.576
Guyung	71	98.854	116	112.748
Kedungprahu	77	79.485	96	92.808
Kendal	106	94.628	109	107.105
Kricak	50	82.860	147	96.950
Legundi	54	90.691	75	107.030
Paron	91	93.450	106	109.643
Tretes	137	87.230	139	104.257
Widodaren	96	96.364	94	113.610
RMSE	**29.404**		**25.201**	
Observation Stations	**2021**		**2022**	
	Actual	**Predicted**	**Actual**	**Predicted**
Gemarang	87	110.283	63	114.557
Guyung	111	119.232	81	123.322
Kedungprahu	103	99.115	115	103.143
Kendal	106	113.156	89	117.045
Kricak	94	103.675	155	108.001
Legundi	100	115.130	150	120.439
Paron	94	117.510	104	122.612
Tretes	93	112.811	106	118.463
Widodaren	86	122.352	88	128.178
RMSE	**19.048**		**34.278**	

Based on the model goodness measure shown in Table 9, the smallest RMSE is observed in 2021 for the 3-year period, with a value of 19.048, compared to the other three periods. Therefore, it can be concluded that the trend surface model generated from max-stable processes with an extremal-t process approach is suitable for use in the next 3 years, based on the extreme values from the 3-month period.

V. CONCLUSIONS AND SUGGESTIONS

The best trend surface model of the extremal-t process identified by the smallest TIC value effectively captures the characteristics of extreme rainfall in Ngawi Regency for the period March 1990 to November 2018. The model indicates that both the mean and variance of extreme rainfall are influenced by latitude, while the shape parameter remains constant under the isotropic assumption, suggesting uniform tail behavior across all observation stations. The return level analysis demonstrates that the highest prediction accuracy is achieved for the 3-year return period, making it the most reliable forecasting horizon for extreme rainfall in the region. Mapping and parameter estimation results further

reveal that several stations, such as Widodaren, exhibit a higher probability of experiencing intense rainfall events, which may elevate localized flood risk. This highlights the importance of targeted preparedness and mitigation efforts, particularly in areas with higher return level estimates.

Strategic focus should remain on enhancing water resource management and implementing region-specific flood mitigation measures to minimize potential damage and support community resilience. The model has the potential to be integrated into regional disaster management systems to improve anticipation of extreme rainfall events. Authorities are encouraged to strengthen water infrastructure planning, improve agricultural adaptation practices, and optimize rainwater utilization. Periodic updates of the model using newer and more detailed datasets, along with the inclusion of relevant environmental covariates, will help maintain its accuracy and operational reliability.

REFERENCES

[1] BMKG, "Prakiraan Musim Hujan 2021/2022 di Indonesia," Jakarta, 2021.

[2] E. Surmaini and A. Faqih, "Kejadian Iklim Ekstrem Dan Dampaknya Terhadap Pertanian Tanaman Pangan Di Indonesia," *Jurnal Sumberdaya Lahan*, vol. 10, no. 2, 2016, doi: 10.2017/jsdl.v10n2.2016.%p.

[3] BMKG, "Leaflet Hidrometeorologi: Mengenal Bencana Hidrometeorologi," 2019, *Jakarta*. [Online]. Available: https://iklim.bmkg.go.id/publikasi-klimat/ftp/brosur/Leaflet%20Hidrometeorologi.pdf

[4] M. G. Donat, A. L. Lowry, L. V. Alexander, P. A. O'Gorman, and N. Maher, "More extreme precipitation in the world's dry and wet regions," *Nat Clim Chang*, vol. 6, no. 5, pp. 508–513, May 2016, doi: 10.1038/nclimate2941.

[5] M. Marzuki *et al.*, "Long-Term Spatial–Temporal Variability, Trends and Extreme Rainfall Events Over Indonesia Based on 43 Years of <scp>CHIRPS</scp> Data," *International Journal of Climatology*, vol. 45, no. 14, Nov. 2025, doi: 10.1002/joc.70107.

[6] A. Kurniadi, E. Weller, J. Salmond, and E. Aldrian, "Future projections of extreme rainfall events in Indonesia," *International Journal of Climatology*, vol. 44, no. 1, pp. 160–182, Jan. 2024, doi: 10.1002/joc.8321.

[7] M. Gilli and E. këllezi, "An Application of Extreme Value Theory for Measuring Financial Risk," *Comput Econ*, vol. 27, no. 2–3, pp. 207–228, May 2006, doi: 10.1007/s10614-006-9025-7.

[8] L. De Haan, "A Spectral Representation for Max-stable Processes," *The Annals of Probability*, vol. 12, no. 4, pp. 1194–1204, 1984, [Online]. Available: http://www.jstor.org/stable/2243357

[9] R. L. Smith, "Max-stable processes and spatial extremes," *Unpublished manuscript*, vol. 205, pp. 1–32, 1990.

[10] T. Opitz, "Extremal t processes: Elliptical domain of attraction and a spectral representation," *J Multivar Anal*, vol. 122, pp. 409–413, Nov. 2013, doi: 10.1016/j.jmva.2013.08.008.

[11] L. Yang, C. L. E. Franzke, and W. Duan, "Evaluation and projections of extreme precipitation using a spatial extremes framework," *International Journal of Climatology*, vol. 43, no. 7, pp. 3453–3475, Jun. 2023, doi: 10.1002/joc.8038.

[12] A. Kurniadi, E. Weller, S. Min, and M. Seong, "Independent ENSO and IOD Impacts on Rainfall Extremes Over Indonesia," *International Journal of Climatology*, vol. 41, no. 6, pp. 3640–3656, May 2021, doi: 10.1002/joc.7040.

[13] E. Y. Shchetinin and N. D. Rassakhan, "Modeling of Extreme Precipitation Fields on the Territoryof the European Part of Russia," *RUDN Journal of Mathematics, Information Sciences and Physics*, vol. 26, no. 1, pp. 74–83, 2018, doi: 10.22363/2312-9735-2018-26-1-74-83.

[14] H. Schellander and T. Hell, "Modeling snow depth extremes in Austria," *Natural Hazards*, vol. 94, no. 3, pp. 1367–1389, Dec. 2018, doi: 10.1007/s11069-018-3481-y.

[15] A. Boluwade, "Stochastic modeling of spatial dependency structures of extreme precipitation in the Northern Great Plains using max-stable processes," *Journal of Water and Climate Change*, vol. 14, no. 9, pp. 3131–3149, Sep. 2023, doi: 10.2166/wcc.2023.187.

[16] S. A. Padoan, M. Ribatet, and S. A. Sisson, "Likelihood-Based Inference for Max-Stable Processes," *J Am Stat Assoc*, vol. 105, no. 489, pp. 263–277, Mar. 2010, doi: 10.1198/jasa.2009.tm08577.

[17] S. Coles, "Classical Extreme Value Theory and Models," 2001, pp. 45–73. doi: 10.1007/978-1-4471-3675-0_3.

[18] E. Omey, F. Mallor, and E. Nualart, "An introduction to statistical modelling of extreme values. Application to calculate extreme wind speeds," 2009.

[19] M. Ribatet, "A user's guide to the SpatialExtremes package," *EPFL, Lausanne, Switzerland*, vol. 200, 2009.

[20] M. Ribatet, "Spatial extremes: Max-stable processes at work," *Journal de la société française de statistique*, vol. 154, no. 2, pp. 156–177, 2013, [Online]. Available: https://www.numdam.org/item/JSFS_2013__154_2_156_0/

[21] R. A. Fisher and L. H. C. Tippett, "Limiting forms of the frequency distribution of the largest or smallest member of a sample," *Mathematical Proceedings of the Cambridge Philosophical Society*, vol. 24, no. 2, pp. 180–190, Apr. 1928, doi: 10.1017/S0305004100015681.

[22] B. Gnedenko, "Sur La Distribution Limite Du Terme Maximum D'Une Serie Aleatoire," *The Annals of Mathematics*, vol. 44, no. 3, p. 423, Jul. 1943, doi: 10.2307/1968974.

[23] A. C. Davison, S. A. Padoan, and M. Ribatet, "Statistical Modeling of Spatial Extremes," *Statistical Science*, vol. 27, no. 2, May 2012, doi: 10.1214/11-STS376.

[24] M. A. Stephens, "EDF Statistics for Goodness of Fit and Some Comparisons," *J Am Stat Assoc*, vol. 69, no. 347, p. 730, Sep. 1974, doi: 10.2307/2286009.

[25] A. Bechler, L. Bel, and M. Vrac, "Conditional simulations of the extremal t process: Application to fields of extreme precipitation," *Spat Stat*, vol. 12, pp. 109–127, May 2015, doi: 10.1016/j.spasta.2015.04.003.

[26] D. Cooley, P. Naveau, and P. Poncet, "Variograms for spatial max-stable random fields," in *Dependence in Probability and Statistics*, P. Bertail, P. Soulier, and P. Doukhan, Eds., New York, NY: Springer New York, 2006, pp. 373–390. doi: 10.1007/0-387-36062-X_17.

[27] L. Anselin, *Spatial econometrics: methods and models*, vol. 4. Springer Science & Business Media, 1988.

[28] P. Asadi, S. Engelke, and A. C. Davison, "Optimal regionalization of extreme value distributions for flood estimation," *J Hydrol (Amst)*, vol. 556, pp. 182–193, Jan. 2018, doi: 10.1016/j.jhydrol.2017.10.051.

[29] E. Aldrian and R. Dwi Susanto, "Identification of three dominant rainfall regions within Indonesia and their relationship to sea surface temperature," *International Journal of Climatology*, vol. 23, no. 12, pp. 1435–1452, Oct. 2003, doi: 10.1002/joc.950.